

Numerical analysis of circular steel tube confined UHPC stub columns

An Le Hoang* and Ekkehard Fehling^a

Faculty of Civil and Environmental Engineering, Institute of Structural Engineering, University of Kassel Kurt-Wolters-Straße 3,
34125, Kassel, Germany

(Received July 2, 2016, Revised December 20, 2016, Accepted December 24, 2016)

Abstract. In this paper, a finite element model (FEM) in ATENA-3D software was constructed to investigate the behavior of circular ultra high performance concrete (UHPC) filled steel tube stub columns (UHPC-FSTCs) under concentric loading on concrete core. The “CC3DNonLinCementitious2User” material type for concrete in ATENA-3D software with some modifications of material laws, was adopted to model for UHPC core with consideration the confinement effect. The experimental results obtained from Schneider (2006) were then employed to verify the accuracy of FEM. Extensive parametric analysis was also conducted to examine the influence of concrete compressive strength, steel tube thickness and steel yield strength on the compressive behavior of short circular UHPC-FSTCs. It can be observed that the columns with thicker steel tube show better strength and ductility, the sudden drop of load after initial peak load can be prevented. Based on the regression analysis of the results from parametric study, simplified formulae for predicting ultimate loads and strains were proposed and verified by comparing with previous analytical models, design codes and experimental results.

Keywords: UHPC; ATENA-3D; finite element model; confinement effect; concrete filled steel tube

1. Introduction

The concrete filled steel tube columns (CFSTCs) have drawn much research attention in civil engineering (Han *et al.* 2014). It is well established that lateral confinement effect provided by the steel tube plays a major role in increasing the compressive strength, deformability, and energy absorption capacity of concrete core, while the local buckling of the steel tube is postponed by the restraining effect of concrete (Johansson 2002 and Han *et al.* 2014). Due to the continuous wrapping of concrete core by steel tube, CFSTCs perform higher stiffness, ductility, strength and fire resistances compared to reinforced concrete columns. Furthermore, the steel tube acts as a permanent formwork, which in turn reduces the cost on transportation and assemblage of columns. These advantages have led to the extensive application of CFSTCs in multi-storey building and bridges (Liew and Xiong 2012).

With developments in concrete technology, research efforts have been directed towards the use of ultra high performance concrete (UHPC) in CFSTCs. It is well known that with a very high compressive strength exceeding of 150 MPa, possibly attaining 250 MPa, UHPC exhibits superior mechanical and durability properties over traditional normal strength concrete (NSC) and high strength concrete (HSC) (Fehling *et al.* 2014). These advantages have been widely exploited for structural members in order to reduce the column size and to achieve the very high loading capacity

(Liew and Xiong 2012). However, the use of UHPC in practice poses difficulties because of the inherently brittle nature of the concrete accompanying with the increase of compressive strength. It was found that steel fiber play little act in improving the compressive ductility of UHPC, so it is necessary to utilize steel tube to alleviate the brittleness of UHPC (Yan and Feng 2008). Although there have been many studies on NSC and HSC filled steel tube columns (NSC-FSTCs and HSC-FSTCs), research on steel tube columns filled with UHPC (UHPC-FSTCs) or ultra high strength concrete (UHSC-FSTCs) remains very limited with only a handful of experimental studies reported (e.g., Tue *et al.* 2004a, Schneider 2006, Yan and Feng 2008, Liew and Xiong 2010, 2012, Guler *et al.* 2013, Chu 2014). In general, UHPC-FSTCs under concentric loading are characterized by very high loading capacity compared to NSC-FSTCs and HSC-FSTCs, but the post-peak behavior is quite brittle with a steep load drop in the load-shortening curves right after the peak load (Liew and Xiong 2010, 2012). Furthermore, the confinement effect in short circular UHPC-FSTCs is less effective in comparison with HSC-FSTCs and NSC-FSTCs, this is due to lower lateral strain of UHPC at high stress level compared with those of NSC and HSC (Tue *et al.* 2004a). As also mentioned by previous researchers, for short circular UHPC-FSTCs under concentric loading on entire section, no significant confinement effect could be developed until the first peak load, thus it is recommended that the confinement effect should be ignored (Yan and Feng 2008, Guler *et al.* 2013, Liew *et al.* 2014).

It was clearly identified that the majority of existing experimental studies have been performed on circular UHPC-FSTCs with the case of concentric loading on both steel tube and concrete core. As suggested by Liew *et al.* (2014) and Xiong (2012), the load should be imposed only

*Corresponding author, Ph.D. Student
E-mail: lehoanganadv@gmail.com

^aProfessor
E-mail: fehling@uni-kassel.de

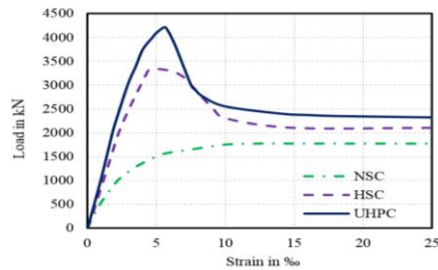


Fig. 1 Load versus vertical strain of short circular CFSTCs loaded on concrete core using NSC, HSC and UHPC (Schneider 2006)

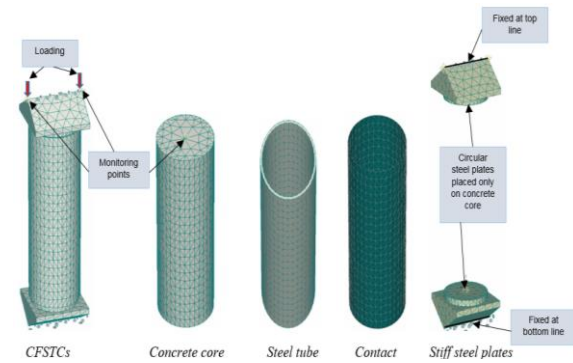


Fig. 2 Mesh and boundary conditions

on the concrete core to achieve the maximum triaxial confinement effect, resulting in the improvement of the ductility and strength of circular UHPC-FSTCs. Tue *et al.* (2004b) pointed out that the abrupt load drop in load-shortening curves of circular UHPCFSTCs can be overcome by sufficient confinement of the steel tube under predominant compression load such as loading on only concrete core. A series of tests on short circular UHPCFSTCs with various steel tube thickness ranging from 2.5 mm to 8 mm under loading on concrete core and loading on entire section were undertaken and reported by Schneider (2006). The results of these tests revealed that short circular UHPC-FSTCs under loading on concrete core experience higher ultimate load and better ductility compared to that under loading on entire section. Furthermore, in Schneider (2006), additional tests on short circular NSC-FSTCs and HSC-FSTCs were also conducted in parallel to get better understanding of difference among circular CFSTCs using various concrete strengths as shown in Fig. 1. Hence, to accelerate the application of UHPC in CFSTCs and to compensate the disadvantages of UHPC core under compression, additional studies on circular UHPC-FSTCs under loading on concrete core should be carried out.

It can be clearly seen that most of numerical studies on CFSTCs have been carried out by using ABAQUS software based on the modification to Concrete Damaged Plasticity Model (CDPM) and the majority of these numerical studies have been focused on the behavior of NSC-FSTCs and HSC-FSTCs. So far, there are few publications devoted to simulating the behavior of UHPC-FSTCs or UHSC-FSTCs (e.g., Schneider 2006, Scholle and Lohaus 2012, Song and Liew 2012, Yang *et al.* 2013, Tao *et al.* 2013). More recently, Tao *et al.* (2013) developed a refined finite element model (FEM) to simulate CFSTCs with a wide range of concrete strengths. A new three-stage model including the strain hardening and softening rule for confined concrete is proposed and adopted in ABAQUS software in combination with calibration some key material parameters in CDPM. The predictions from the new FEM were in good agreement with the test results of CFSTCs using concrete strength up to 163 MPa presented by Liew *et al.* (2010), indicating that the new FEM proposed by Tao *et al.* 2013 is capable of modeling CFSTCs using UHSC. Similarly, Song and Liew (2012) introduced a simulation model for UHSC-FSTCs under static loads based on the modification to the uniaxial concrete compressive

stress-strain relationship with considering the confinement effect provided by steel tube. An *et al.* (2016) presented a numerical model in ATENA-3D for short circular CFSTCs using three types of concrete including NSC, HSC and UHPC. Currently, to the authors' knowledge, apart from some numerical studies on the behavior of UHPC-FSTCs or UHSC-FSTCs as mentioned above, there is no comprehensive FEM concerned with this subject.

ATENA-3D software program developed by Cervenka Consulting is well-known as a useful tool for modelling of concrete structures. By using ATENA-3D, the behavior of structural member could be predicted not only at ultimate load but also throughout the complete loading history. Unlike NSC and HSC which have well defined material models, no standard model for UHPC is implemented in ATENA-3D; for this reason, the concrete material type "CC3DNonLinCementitious2User" should be used for modelling the behavior of UHPC in CFSTCs because it allows the user to define their own material model laws, beside that the confinement effect is also automatically considered in this model (Cervenka *et al.* 2013).

From the issues discussed above, it can be broadly concluded that the understanding of the fundamental behavior of UHPC-FSTCs is not sufficient owing to the lack of experimental and numerical research on this type of composite columns. Especially, there is not enough information about the behavior of UHPC-FSTCs subjected to the load on only concrete core. Moreover, it was argued that although experimental tests play a significant role in the research, they are quite expensive and time consuming, particularly for UHPC. Hence, numerical studies are much needed to provide supplementary information to the experiments and to enable further parametric studies, thus contributing to the prediction of the behavior of structure without testing.

To address the aforementioned research gaps, in this paper, the new FEM for short circular UHPC-FSTCs using UHPC with compressive strength higher than 150 MPa under loading on concrete core were developed in ATENA-3D software and calibrated with experimental results obtained from Schneider (2006) to validate their accuracy. Extensive parametric studies were then conducted by using established FEM to point out the influence of concrete compressive strength, steel tube thickness, steel yield strength on the strength and the ductility of the columns. It should be noted that, in this study, UHPC without fibers

was considered in modelling. Finally, simplified formulae were proposed to predict the ultimate loads and corresponding strains.

2. Finite element modelling in ATENA-3D

2.1 Finite element type and mesh

In this study, 3D solid Tetrahedral elements (CCIsoTetra) with reduced integration (4 nodes) were employed for steel tube, concrete core and stiff steel plates as shown in Fig. 2. The global element size was determined to be 30 mm to obtain the best results and the least possible errors. The mesh compatibility was requested on the contact between steel tube and concrete core, concrete core and stiff steel plate. Furthermore, the interface elements (CCIsoGap) were chosen to analyze the contact between steel tube and concrete core.

2.2 Boundary conditions and load application

To minimize the influence of end conditions on circular CFSTCs, two steel plates have been placed at both ends of a column in the experimental set up. If no stiffening method is used, local buckling of the steel tube is more likely to be initiated at the ends, which may affect to the performance of the specimen. Consequently, in FEM, two stiff steel plates were modelled at each end of concrete core to reflect experimental boundary conditions and the contact between the surface of steel stiff plates and the surface of concrete core were defined as “perfect connection”.

With the effort to achieve identical boundary conditions and geometry between full 3D model and experimental set up, the stiff steel plates with triangular shape were chosen as shown in Fig. 2, representing the loading mechanism as in the actual test and preventing unrealistic deformation as well as unequal loading distribution. The material type of stiff steel plates was defined as 3D Elastic Isotropic material (CC3D ElastIsotropic) with extremely large elastic modulus of 2.10^6 MPa and the Poisson’s ratio of 0.3. The top line of stiff steel plate was fixed against all degrees of freedom except for the direction of the applied load, while the bottom line of stiff steel plate was fixed in all direction as shown in Fig. 2.

In ATENA-3D, the load is increased simultaneously by displacement control and the Newton-Raphson iteration method is used for solving nonlinear equations (Cervenka *et al.* 2013). Thus, two prescribed deformations were placed at two monitoring points on the top line of upper stiff steel plate as illustrated in Fig. 2. Through these two monitoring points, a graph of load-displacement relationship was generated in analysis step and also fully observed in post-processor tool of ATENA-3D. Another monitoring point in the middle of top surface of concrete core was also used to record the displacement of concrete core (as seen in Fig. 2) and the vertical strain of concrete core was derived by the ratio of this displacement to concrete core length.

2.3 Constitutive models of steel tube

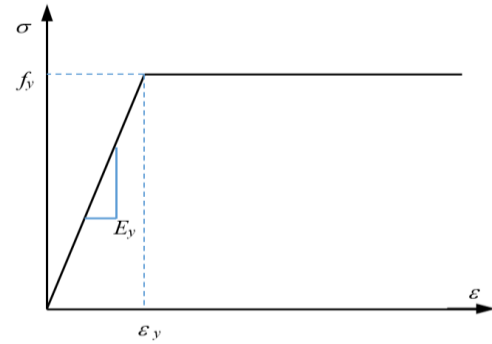


Fig. 3 Elastic-perfectly plastic model for steel tube

The constitutive behavior of the steel tube was assumed to follow the elastic-perfectly plastic material model as shown in Fig. 3. The Von-Mises yield criterion was also applied for steel tube due to biaxial stress state of steel in yield condition. Hence, in ATENA-3D, steel tube was modelled using material type “CC3DBilinearSteelVonMises” with the yield stress f_y and the elastic modulus E_y of 2.10^5 MPa for normal strength steel tube. The Poisson’s ratio for steel tube was taken as 0.3, this value has been used widely in numerical simulation.

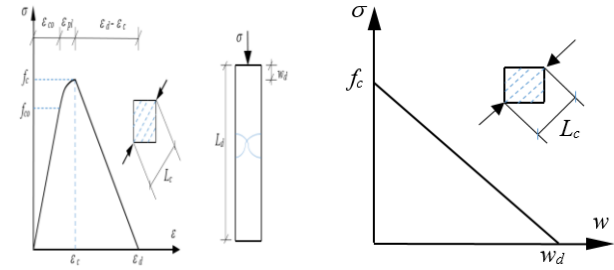
2.4 Constitutive models of UHPC core

The concrete core can be modeled by using material type “CC3DNonlinCementitious2User” in ATENA-3D. The hydrostatic failure criterion (Menétrey-Willam plasticity function) was adopted in order to evaluate the hardening/softening behavior of concrete in compression. On the other hand, for concrete cracking in the tensile region, Rankine failure criterion was employed. The combination of these two models in “CC3DNonlinCementitious2User” material type allows for the simulation of concrete cracking, crushing under high confinement (Cervenka *et al.* 2013). Since the composite action between concrete core and steel tube, the confinement effect provided by steel tube causes concrete core to behave in a triaxial compressive stress, the failure of concrete core is dominated by the compressive failure surface expanding with increasing hydrostatic pressure. In order to describe this triaxial strength of concrete as mentioned, the hardening/softening plasticity model including three independent stress invariants (ζ, ρ, θ) based on Menétrey-Willam failure surface is used. The failure surface F_{3P}^p of Menétrey-Willam is expressed by the equations as follows

$$F_{3P}^p = \left[\sqrt{1.5} \cdot \frac{\rho}{f_c} \right]^2 + m \left[\frac{\rho}{\sqrt{6} \cdot f_c} r_1(\theta, \varepsilon) + \frac{\xi}{\sqrt{3} f_c} \right] - c = 0 \quad (1)$$

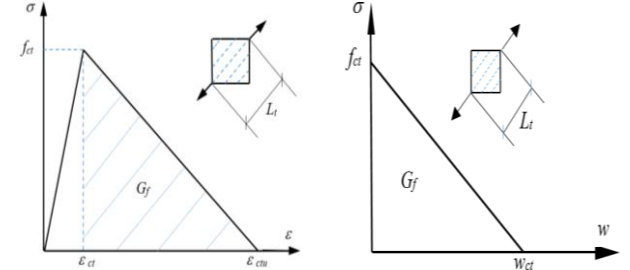
$$m = 3 \cdot \frac{f_c^2 - f_{ct}^2}{f_c f_{ct}} \cdot \frac{e}{e+1} \quad (2)$$

$$r_1(\theta, e) = \frac{4 \cdot (1 - e^2) \cdot \cos^2 \theta + (2e - 1)^2}{2 \cdot (1 - e^2) \cdot \cos \theta + (2e - 1) \cdot \left[4 \cdot (1 - e^2) \cdot \cos^2 \theta + 5 \cdot e^2 - 4 \cdot e \right]^{\frac{1}{2}}} \quad (3)$$



(a) Complete stress-strain (b) Softening law in of UHPC in compression compression

Fig. 4 Diagram of UHPC core in compression



(a) Complete stress-strain (b) Linear crack opening in of UHPC in tension tension

Fig. 5 Diagram of UHPC core in tension

Where (ξ, ρ, θ) are Heigh-Westergaard coordinates, $r_1(\theta, e)$ is the elliptic function, m is the friction parameter, f_c and f_{ct} are the uniaxial compressive strength and the uniaxial tensile strength, respectively. e is defined as the eccentricity to describe the roundness of the failure surface and ranged from 0.5 to 1.0. In this study, for UHPC, deriving from the ratio between the equibiaxial (f_{bc}) to uniaxial compressive concrete strength (f_c) ($f_{bc}/f_c=1.1$), e was taken as 0.5.

It can be seen that the material type “CC3DNonlinCementitious2User” allows the user to define his own material model laws. The main features of these laws are as follows:

- Tension function (including post cracking softening behavior)
- Diagram for compression (including post-peak branch behavior)
- Strength reduction due to cracking
- Shear function
- Shear strength reduction due to cracking
- Tension-compression function

2.4.1 Material law for UHPC under compression

The complete stress-strain curve for UHPC in compression is given in Fig. 4(a). The ascending branch of stress-strain curve comprises three parts, linear part up to a compressive strength f_{co} , hardening part up to ultimate strength f_c and softening part. Based on previous test results (e.g., Schneider 2006, Fehling *et al.* 2014, Xiong 2012), the behavior of UHPC without fibers in compression can be modeled as linear elastic up to 80% of peak stress ($f_{co}=0.8 f_c$) and the Poisson's ratio is taken as 0.2. For defining the hardening part, the plastic strain ε_{pl} is used in the diagram of UHPC in compression. The plastic strain ε_{pl} represents the strain value, after which strain localization can be expected and it can be calculated as follows

$$\varepsilon_{pl} = \varepsilon_c - \varepsilon_{co} = \varepsilon_c - \frac{f_c}{E_c} \quad (4)$$

Where ε_c is the strain value at ultimate stress f_c , and E_c is the elastic modulus. The values of ε_c and E_c (for UHPC without fibers) can be determined by the following equations proposed by Schneider (2006) and Fehling *et al.* (2014)

$$\varepsilon_c = 0.00083 f_c^{0.276} \quad (5)$$

$$E_c = 10200 \cdot f_c^{1/3} \quad (6)$$

It should be noted that, in ATENA-3D, the softening law of concrete in compression is based on the displacement. The softening law of UHPC without fibers in compression is assumed linearly descending as demonstrated in Fig. 4(b). The end point of the softening curve is defined by means of the plastic displacement w_d . To obtain identical descending curve between FEM and experimental tests, the value of $w_d=0.4$ mm for UHPC was chosen. For determining the descending branch in diagram of compression and reducing the dependency on finite element mesh, the limit compressive strain ε_d at the zero stress is derived from the plastic displacement w_d and the band size L_c during failure in compression

$$\varepsilon_d = \varepsilon_c + \frac{w_d}{L_c} \quad (7)$$

2.4.2 Material law for UHPC under tension

Fig. 5(a) illustrates the complete stress-strain curve of UHPC without fibers in tension. The ascending branch in tension before cracking is assumed to be linear-elastic up to tensile strength f_{ct} . The corresponding strain ε_{ct} at f_{ct} is calculated as follow

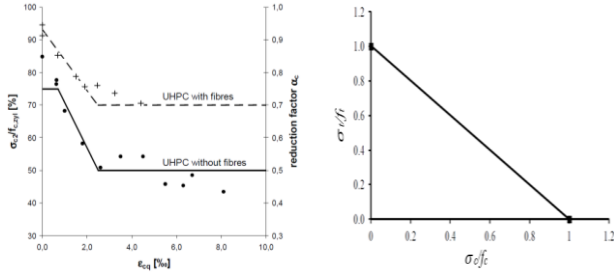
$$\varepsilon_{ct} = \frac{f_{ct}}{E_c} \quad (8)$$

According to Fehling *et al.* 2014, for UHPC, f_{ct} can be expressed by the relationship with f_c as follow

$$f_{ct} = 0.3 \cdot (f_c)^{2/3} \quad (9)$$

In order to determine the tension function of UHPC without fibers after cracking in ATENA-3D, the linear crack opening law can be assumed as shown in Fig. 5(b). According to Leutbecher (2008), for UHPC without fibers and using coarse aggregate, the fracture energy G_f could be taken as 95 N/m and the characteristic length l_{ch} is equal to 80.6 mm. Hence, the strain corresponding to zero stress in the descending branch of tension after cracking ε_{ctu} is calculated as follows

$$\varepsilon_{ctu} = \frac{w_{ct}}{L_t} \quad (10)$$



(a) Strength reduction due to cracking based on Fehling *et al.* (2008) (b) Reduction of tensile strength due to lateral compression based on Speck and Curbach (2011)

Fig. 6 Other laws of UHPC adopted in ATENA-3D

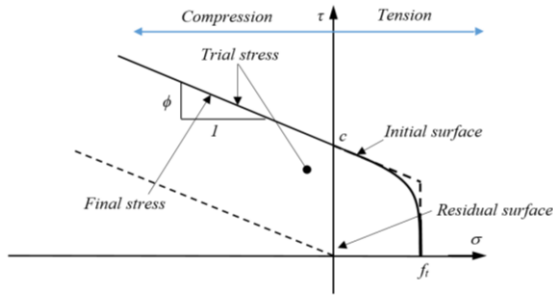


Fig. 7 Failure surface for interface element (Cervenka *et al.* 2013)

Where w_{ct} is defined as the crack opening at the complete release of stress and given by the equation

$$w_{ct} = \frac{2 \cdot G_f}{f_{ct}} \quad (11)$$

Where L_t is the crack band size calculated as a size of the element projection in the crack direction.

2.4.3 Other laws for UHPC

In the case of UHPC, some laws should be newly defined by previous assumptions of some researchers due to different characteristics in uniaxial, biaxial or triaxial behavior compared to NSC, HSC. In this study, the compressive strength reduction due to lateral tensile strain was assumed to follow the results obtained by Fehling *et al.* (2008) for UHPC without steel fibers as shown in Fig. 6(a) and the effect of lateral compression on the tensile strength of UHPC was estimated based on the experimental results conducted by Speck and Curbach (2011) as shown in Fig. 6(b).

2.5 Modelling of interfaces between steel tube and concrete core

The “CC3DInterface” material type in ATENA-3D was used to model the contact between steel and concrete core. The interface material is based on Mohr-Coulomb criterion as shown in Fig. 7 (Cervenka *et al.* 2013). The constitutive relation for a general 3D-dimensional case is given in terms of tractions on interface planes and relative sliding and opening displacements and it is given as follow

Table 1 Dimensions and material properties of short circular UHPC-FSTCs in the tests by Schneider (2006)

Specimen ID	Outer Diameter D (mm)	Steel tube thickness t (mm)	Column length L (mm)	Concrete strength f_c (MPa)	Steel yield strength f_y (MPa)
NB2.5	164.2	2.5	652	166.8	377
NB3.0	189.0	3.0	756	166.8	398
NB4.0	168.6	3.9	648	174.2	363
NB4.8	169.0	4.8	645	176.7	399
NB5.0	168.7	5.2	645	170.5	405
NB5.6	168.8	5.7	650	173.4	452
NB8.0	168.1	8.1	645	174.9	409

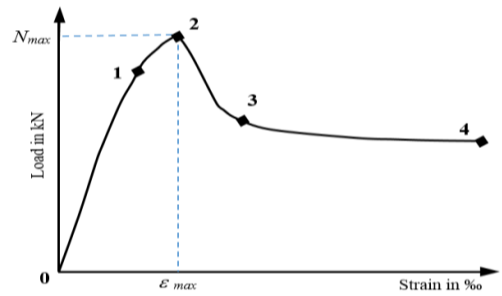


Fig. 8 Load versus vertical strain curve of short circular UHPC-FSTCs loaded on concrete core

$$\begin{Bmatrix} \tau_1 \\ \tau_2 \\ \tau_3 \end{Bmatrix} = \begin{bmatrix} K_{tt} & 0 & 0 \\ 0 & K_{tt} & 0 \\ 0 & 0 & K_{nn} \end{bmatrix} \begin{Bmatrix} \Delta v_1 \\ \Delta v_2 \\ \Delta u \end{Bmatrix} \quad (12)$$

Where τ is shear stress in direction x and y, while σ is normal stress

Δv_1 and Δv_2 are relatively displacements on surface and Δu is relatively opening of contact

K_{tt} is initial elastic shear stiffness and K_{nn} is initial elastic normal stiffness. The values of K_{tt} and K_{nn} are estimated from the equations as follows

$$K_{nn} = \frac{E}{t}, K_{tt} = \frac{G}{t} \quad (13)$$

Where E and G are minimal elastic modulus and shear modulus, respectively, of the surrounding material; and t is the width of interface zone.

There are two additional stiffness values that need to be specified in the ATENA-3D input. They are denoted as $K_{nn(min)}$, $K_{tt(min)}$. These values are used only for numerical purposes after the failure of the element in order to preserve the positive definiteness of the global system of equations. The K_{nn} and K_{tt} get extremely high values (approaching to infinity) because the width of interface zone t between concrete core and steel tube is approaching to zero value (Cervenka *et al.* 2013). Therefore, according to the recommendation in Pryl and Cervenka (2015), the initial stiffnesses K_{nn} and K_{tt} can be determined by the equation

$$K_{nn} = K_{tt} = \frac{E_c}{s} \cdot 10 \quad (14)$$

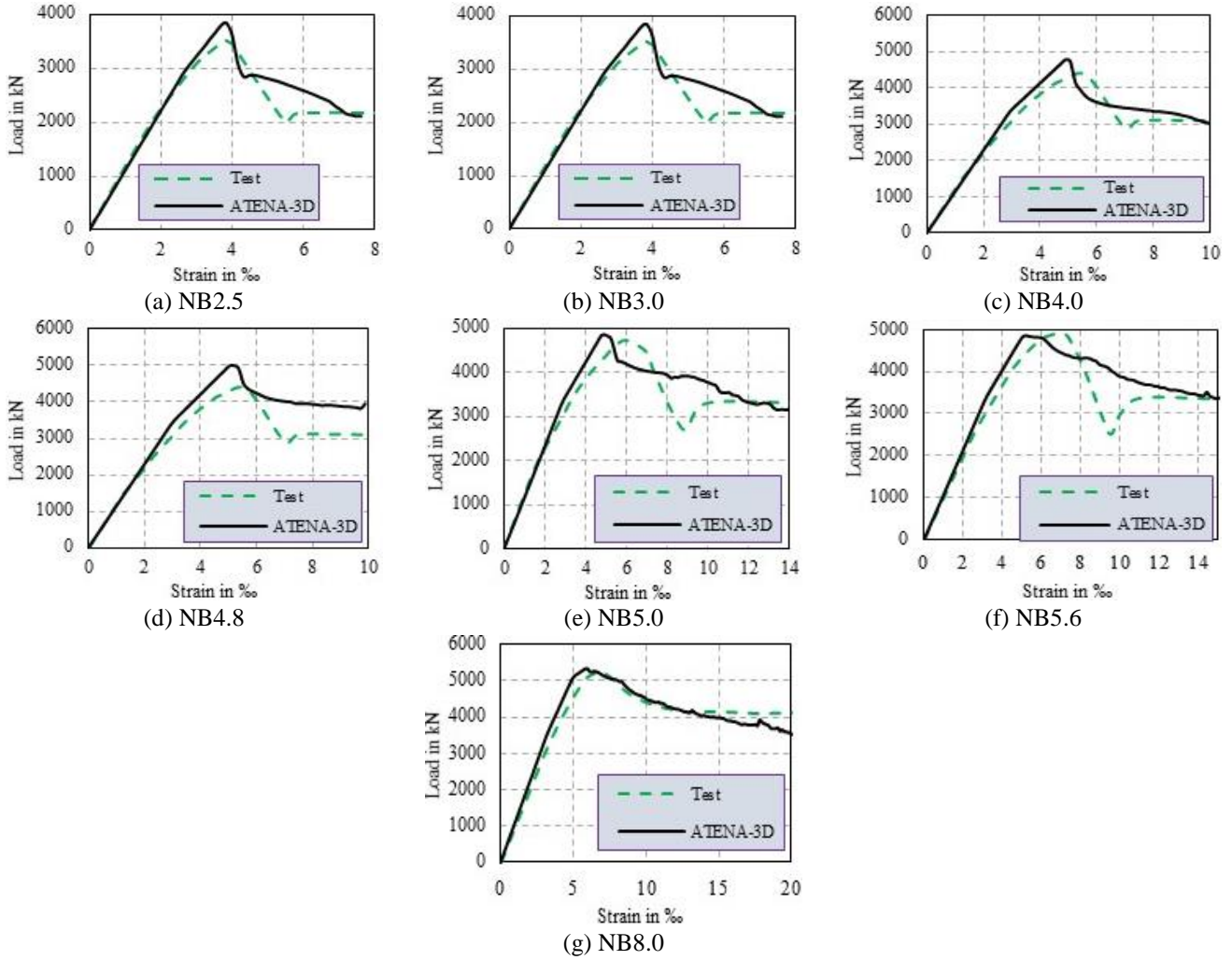


Fig. 9 Comparisons of L-S curves between FEM in ATENA-3D and test results by Schneider (2006)

Where E_c is the elastic modulus of UHPC core (in Pa), s is finite element size of concrete core (in m).

As also suggested in Pryl and Cervenka (2015), the residual stiffness $K_{m(min)}$, $K_{t(min)}$ for numerical purposes are about 0.001 times of the initial stiffness values K_m , K_t , respectively.

The frictional properties of the interface material type in ATENA-3D are defined by shear cohesion c and the friction coefficient ϕ . The failure surface corresponding to Mohr-Coulomb criterion can be described by the following equations (Cervenka *et al.* 2013)

$$|\tau| \leq c - \sigma \cdot \phi, \sigma \leq 0 \quad (15)$$

$$\tau = \tau_0 \sqrt{1 - \frac{(\sigma - \sigma_c)^2}{(f_t - \sigma_c)^2}}, \tau_0 = \frac{c}{\sqrt{1 - \frac{\sigma_c^2}{(f_t - \sigma_c)^2}}}, \sigma_c = -\frac{f_t^2 \cdot \phi}{c - 2 \cdot f_t \cdot \phi}, 0 \leq \sigma \leq f_t \quad (16)$$

$$\tau = 0, \sigma > f_t \quad (17)$$

Where f_t is tensile strength on the surface. It is also recommended to set the interface tensile strength f_t to be

Table 2 Comparisons of ultimate loads and corresponding strains between FEM and test results by Schneider (2006)

Specimen ID	N_{EXP} (kN)	N_{FEM} (kN)	N_{FEM}/N_{EXP}	ϵ_{EXP} (‰)	ϵ_{FEM} (‰)	$\epsilon_{FEM}/\epsilon_{EXP}$
NB2.5	3501	3480	0.99	3.80	3.83	1.01
NB3.0	4837	5220	1.08	4.22	4.07	0.96
NB4.0	4216	4780	1.13	5.57	4.15	0.75
NB4.8	4330	4690	1.08	5.67	4.46	0.79
NB5.0	4751	4850	1.03	5.99	4.92	0.82
NB5.6	4930	4860	0.99	6.84	5.19	0.76
NB8.0	5254	5340	1.02	6.84	5.83	0.85
Mean Value			1.046			0.848
Coefficient of Variation (COV)			0.052			0.120

between 1/2 and 1/4 of the tensile strength of the weaker material next to the interface ($f_t = 1/2 \cdot f_{cr} - 1/4 \cdot f_{ct}$), and the interface cohesion c is suggested to be set to 1-2 times f_t ($c = 1 \cdot f_t - 2 \cdot f_t$) (Pryl and Cervenka 2015).

For short circular CFSTCs, values of friction coefficients between concrete and steel tube ranging from 0.1 to 0.6 have been used by different researchers (Tao *et al.* 2013). In this study, the friction coefficient was taken as 0.4

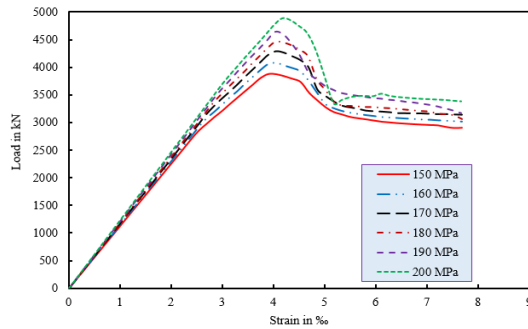


Fig. 10 L-S curves of the columns with different concrete strengths

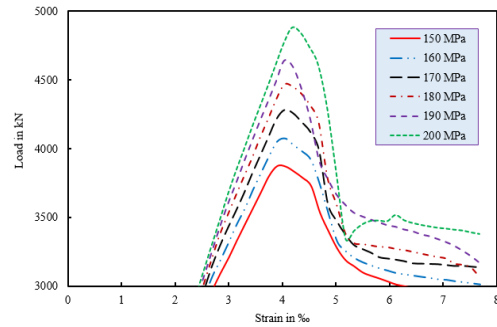


Fig. 11 Detail of elastic-plastic part and abrupt load drop after peak load in L-S curves

to ensure the convergence.

3. Verification of FEM

The dimensions and material properties of short circular UHPC-FSTCs in the tests by Schneider (2006) as illustrated in Table 1 were used for FEM in ATENA-3D. The precision of FEM was judged by comparing the load versus vertical strain (L-S) curves as shown in Fig. 9 and the values of ultimate load and corresponding strain as shown in Table 2 obtained from FEM against the experimental results presented by Schneider (2006).

Generally, the complete L-S curves of short circular UHPC-FSTCs loaded on concrete core can be divided into four phases based on the test results by Schneider (2006) as depicted in Fig. 8. The first phase (0-1) is mainly a linear-elastic response controlled by the stiffness of unconfined UHPC column, where steel tube and UHPC core work independently without the confinement effect. The second phase (1-2) is named as elastic-plastic stage where the confinement effect provided by steel tube is generated owing to the larger Poisson's ratio of UHPC core compared to that of steel tube. However, it can be observed that the second phase is quite short stage, thus the loading in ascending branch increases straightly up to the peak load (N_{max}) and then it drops down. The third phase (2-3) in the descending branch performs the sudden drop of loading due to the inherent brittleness of UHPC at high stress and then followed by the fourth phase (3-4), where the L-S curve is approximately horizontal and the column exhibits excellent ductility.

As can be seen in Fig. 9, the FEM in ATENA-3D predicted very well in both elastic and plastic regions of L-S curves. In addition, the general shape of the complete L-S curves obtained from ATENA-3D exhibited the same stages in comparison with the test results by Schneider (2006). It has been also demonstrated by both ATENA-3D and the test results that thinner steel thickness leads to rapid load drop after the peak load, while the columns with thicker steel thickness such as specimen NB8.0 show a gradual softening process in the post-peak region. This may attributed to the fact that the abrupt load drop of UHPC core can be impeded by the sufficient confinement from steel tube when increasing steel thickness or some other parameters such as yield strength of steel tube and the confinement index.

In terms of the prediction accuracy of ultimate loads (N_{max}) and corresponding strains (ε_{max}), it is evident from Table 2 that the FEM in ATENA-3D gave very reasonable predicted values compared to the measured values in Schneider (2006) with the largest difference in ultimate loads and corresponding strains between the FEM and the test results of approximately 4.6% and 15.2%, respectively.

Based on this verification, it can be concluded that the FEM established in ATENA-3D is reliable to conduct further parametric studies so as to analyze the mechanical performance of short circular UHPC-FSTCs.

4. Parametric study

Some basic parameters including diameter to thickness ratio (D/t), concrete strength (f_c), steel yield strength (f_y) have significant impact on the mechanical behavior of short circular UHPC-FSTCs under loading on concrete core. However, experimental investigation on the effect of all these parameters is practically difficult, since it is an extremely expensive and time consuming process, particularly for UHPC. To date, to the authors' knowledge, except for the tests conducted by Schneider (7 columns) and Xiong (2 columns), there has been no published research available on circular UHPC-FSTCs under loading on concrete core yet (UHPC with minimum cylinder compressive strength of 150 MPa). Hence, it is necessary to provide more data to get better understanding of the effect of these parameters to the compressive behavior for this type of column. Once the present FEM in ATENA-3D was validated, it allows a comprehensive parametric study with taking into account a wide range and combination of these parameters to be investigated.

A total of 14 columns were considered to analyze the effect of t , f_c and f_y on the strength and the ductility of short circular UHPC-FSTCs under loading on concrete core. These columns were divided into 3 groups in order to distinguish among the investigated parameters, and given as follows:

- Group 1 (Investigation on the effect of f_c) consisted of 6 columns having outer diameter (D) of 168.3 mm, steel thickness (t) of 4.0 mm, length (L) of 640 mm, steel yield strength (f_y) of 350 MPa and cylinder compressive strength of UHPC (f_c) of 150, 160, 170, 180, 190, 200 MPa.
- Group 2 (Investigation on the effect of t) comprised 4

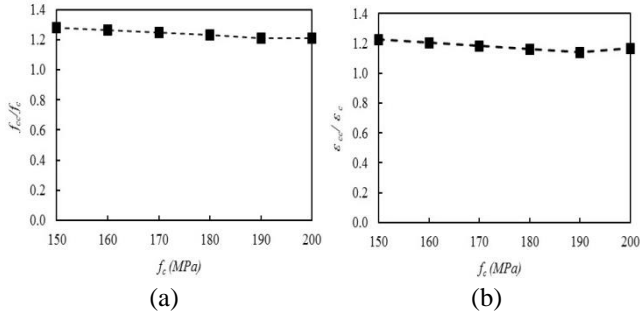


Fig. 12 The relationships: (a) f_{cc}/f_c and (b) $\varepsilon_{cc}/\varepsilon_c$

columns with $D=168.3$ mm, $L=640$ mm, $f_c=160$ MPa, $f_y=350$ MPa, but various steel thicknesses (t) equal to 4, 6, 8, 10 mm. The ratio of D/t covered a range of values between 16.83 and 42.08.

- Group 3 (Investigation on the effect of f_y) included 4 columns with $D=168.3$ mm, $L=640$ mm, $f_c=160$ MPa, $t=4$ mm, but various steel yield strengths (f_y) of 235, 345, 390, 420 MPa.

Overall, it is revealed from the FEM results of these 14 columns that the shape of L-S curves of all columns are observed to be similar to the general curves as described in Fig. 8.

4.1 Effect of concrete strength (f_c)

Fig. 10 shows the L-S curves of short circular UHPC-FSTCs loaded on concrete core of Group 1 with various concrete compressive strengths ranging between 150 MPa and 200 MPa, while Fig. 11 depicts the hardening and the softening part with an abrupt load drop after the first peak load. The results indicate that increasing UHPC compressive strength results in small increase of the initial stiffness, the ultimate load and strain. However, the hardening part of columns using higher compressive strength is more linear than smaller ones. The ultimate load of composite columns increases with an average rate of approximately 5% when the increment of concrete compressive strength is 10 MPa. In addition, the column using higher compressive strength exhibits steeper sudden load drop after the first peak load. For instance, the columns using UHPC with compressive strengths of 190 and 200 MPa shows different softening branch compared to that of other columns, where the second peak load is much smaller than the first peak load. On the other hand, after the first peak load, the softening branch for the columns using compressive strengths of 150, 160, 170, and 180 MPa are almost parallel to each other. This observation can be attributed to the fact that the increase in the concrete strength leads to increased concrete brittleness. Therefore, it can be concluded that the axial ductility of columns decreases moderately with an increase in the UHPC compressive strength, while there is no significant enhancement of strength.

To investigate the effect of concrete strength to the confinement degree, the relation f_{cc}/f_c versus f_c and $\varepsilon_{cc}/\varepsilon_c$ versus ε_c (where f_{cc} and ε_{cc} are the confined compressive strength and corresponding strain, respectively) were

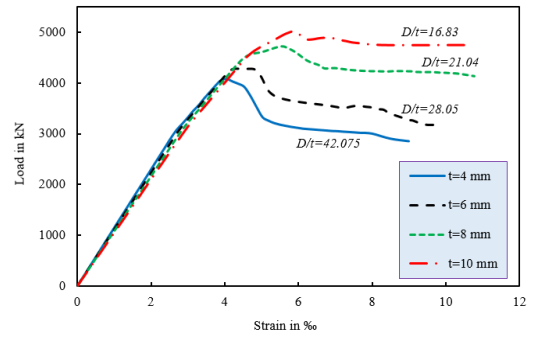


Fig. 13 L-S curves of the columns with various steel thicknesses

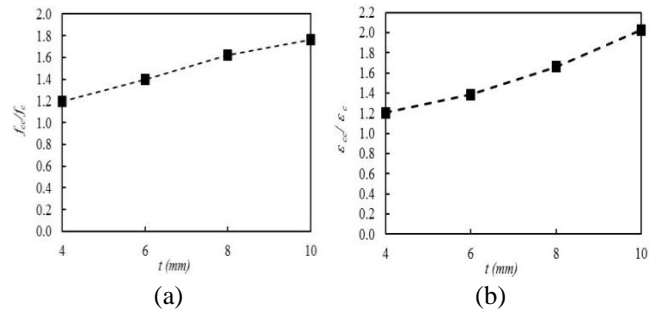


Fig. 14 The relationships: (a) f_{cc}/f_c - t and (b) $\varepsilon_{cc}/\varepsilon_c$ - t

plotted in Fig. 12(a)-(b). It is evident from Fig. 12 that the confinement effectiveness decreases slightly with the increase of unconfined concrete compressive strength ranging between 150 and 200 MPa.

4.2 Effect of steel thickness (t)

The L-S curves of short circular UHPC-FSTCs loaded on concrete core of Group 2 with steel thicknesses of 4, 6, 8, and 10 mm and various D/t ratios are presented in Fig. 13. It is shown in Fig. 13 that increasing steel tube thickness from 4 mm to 10 mm leads to a significant increase in the ultimate load and corresponding strain. On average, when the increment of steel thickness is 2 mm, the ultimate load increases by 10%, while there is an increase of 15%-22% in the strain at ultimate load. Furthermore, as can be seen in Fig. 13, the columns with thinner steel thickness exhibit a rapid load drop after the initial peak load, whereas the columns with thicker tube experience a slight load drop. Similarly, the slope of softening branch of the columns with thinner tube is found to be steeper than that with thicker one. From these observations, it can be stated that the thickness of steel tube has great effect to the behavior of short circular UHPC-FSTCs loaded on concrete core. The pronounced improvement of the ultimate load, corresponding strain, and the ductility is observed with the increase in steel thickness.

The influence of steel thickness on the confinement degree is shown in Figs. 14(a)-(b) by the relationships between f_{cc}/f_c and the steel thickness t ; $\varepsilon_{cc}/\varepsilon_c$ and the steel thickness t . From Figs. 14(a)-(b), it can be seen that the confinement effectiveness increases significantly with the increase in steel tube thickness.

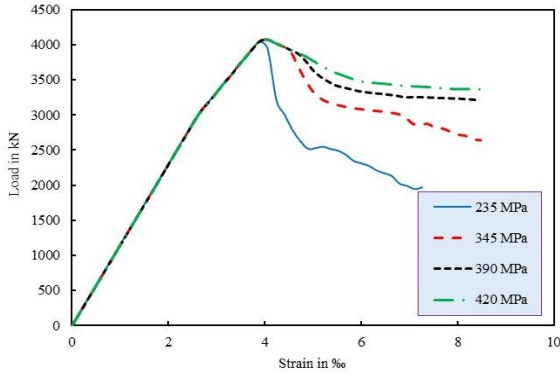


Fig. 15 L-S curves of the columns with various steel yield strengths

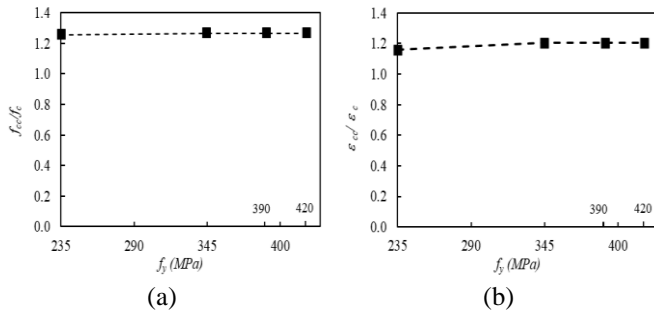


Fig. 16 The relationships: (a) $f_{cc}/f_c - f_y$ and (b) $\epsilon_{cc}/\epsilon_c - f_y$

4.3 Effect of steel yield strength (f_y)

Fig. 15 demonstrates the L-S curves of short circular UHPC-FSTCs loaded on concrete core of Group 3 with steel yield strengths of 235, 345, 390 and 420 MPa. As shown in the Fig. 15, there is no change in the initial stiffness, the ultimate load and corresponding strain with increasing the yield strength of steel tube. However, the main difference among these columns is the softening branch. The column using steel yield strength of 235 MPa performs a rapid load drop after the first peak load, while other columns exhibit slight load drop. Moreover, the softening branch is observed to be steeper with smaller steel yield strengths. Therefore, it can be indicated that there is only an enhancement of ductility with increasing the steel yield strength.

Figs. 16(a)-(b) shows the relationship between f_{cc}/f_c and ϵ_{cc}/ϵ_c and f_y . As can be seen, there is no increase in the confinement effectiveness with using higher steel yield strength compared to that with smaller ones.

4.4 Simplified formulae to predict the ultimate load (N_u) and corresponding strain (ϵ_{cc})

According to Yu *et al.* (2010) and Johansson (2002), the sectional capacity of circular CFSTCs loaded on concrete core is mainly affected by the confinement index ξ given as follows

$$\xi = \frac{A_s \cdot f_y}{A_c \cdot f_c} \quad (18)$$

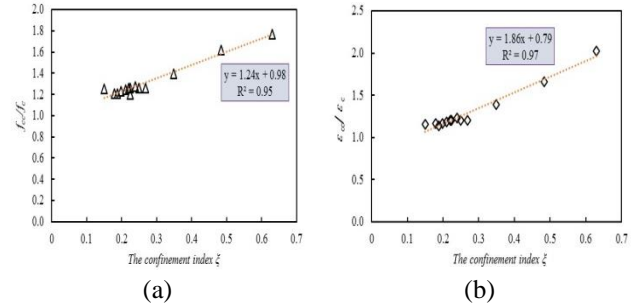


Fig. 17 The relationships: (a) $f_{cc}/f_c - \xi$ and (b) $\epsilon_{cc}/\epsilon_c - \xi$

Where A_s is the cross-sectional area of steel tube, A_c is the cross-sectional area of concrete.

The confinement index ξ is used to determine the combined influences of steel yield strength, concrete compressive strength, and outer diameter of steel tube, as well as steel thickness. It has been found that some formulae for estimating both ultimate load and corresponding strain of circular CFSTCs were built based on the confinement index ξ , such as Han *et al.* (2005), Yu *et al.* (2010). This point of view has motivated the authors to develop simplified formulae by using the results of all columns in parametric study from FEM. Therefore, in this study, simplified formulae obtained from the regression analysis of the relationships between f_{cc}/f_c and the confinement index ξ ; ϵ_{cc}/ϵ_c and the confinement index ξ were proposed to predict the ultimate loads and corresponding strains of short circular UHPC-FSTCs under loading on concrete core.

The ratios of f_{cc}/f_c and ϵ_{cc}/ϵ_c are plotted against the confinement index ξ in Figs. 17(a)-(b). The regression coefficient R^2 has the values of 0.95 and 0.97, respectively, thus indicating a very strong correlation. As a consequence, the formulae for f_{cc} and ϵ_{cc} can be expressed as follows

$$f_{cc} = (0.98 + 1.24 \cdot \xi) \cdot f_c \quad (19)$$

$$\epsilon_{cc} = (0.79 + 1.86 \cdot \xi) \cdot \epsilon_c \quad (20)$$

Moreover, f_{cc} can be defined through the ratio of ultimate load to concrete cross-sectional area, which is given by the following equation

$$f_{cc} = \frac{N_u}{A_c} \quad (21)$$

Thus, the ultimate load of short circular UHPC-FSTCs under loading on concrete core can be easily determined by the following equation

$$N_u = (0.98 + 1.24 \cdot \xi) \cdot A_c \cdot f_c \quad (22)$$

It should be noted that the validity of Eqs. (19)-(20) is: $f_y = 235-420$ MPa, $f_c = 150-200$ MPa, $\xi = 0.1-0.7$.

The ultimate loads and corresponding strains of all tested columns in Table 1 were calculated by using the present prediction and previous analytical models assumed by O'Shea and Bridge (2000), Johansson (2002), and Hatzigeorgiou (2008), as well as some design codes

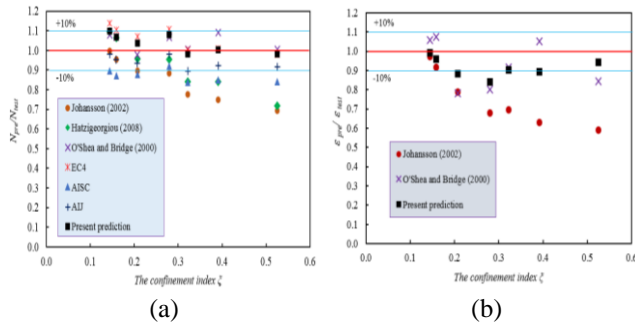


Fig. 18 The ratio of N_{pre}/N_{test} , $\varepsilon_{pre}/\varepsilon_{test}$ versus the confinement index ζ

including EC4 (2004), AISC (2005), AIJ (2001). In order to verify the present formulae, the ratios of predicted values (N_{pre} and ε_{pre}) to the measured values (N_{test} and ε_{test}) in the tests by Schneider (2006) are shown in Figs. 18(a)-(b). It can be observed from Figs. 18(a)-(b) that the present formulae provide reasonable predictions with the largest difference of 10% and 15% for the ultimate loads and strains, respectively, compared to test results. Furthermore, the present formulae show better predictions with the increase in the confinement index ζ .

5. Conclusions

The main objective of this study is to present a FEM of short circular UHPC-FSTCs under loading on concrete core, where the cylinder compressive strengths of UHPC without fibers are higher than 150 MPa. The following conclusions can be drawn within the limitations of the research work in this study:

- The FEM in ATENA-3D successfully predicted the behavior of short circular UHPC-FSTCs under loading on concrete core. The complete L-S curves, ultimate loads and corresponding strains obtained from FEM were in good agreement with the measured results by Schneider (2006). Hence, the FEM in ATENA-3D can be reliably used to analyze the mechanical performance of short circular UHPC-FSTCs under loading on concrete core in the future in order to save time and cost of experimental works.

- The parametric study reveals that the increase in concrete strength of UHPC leads to small increase of ultimate loads and strains, but slightly decreasing the confinement effectiveness. The ductility of columns is moderately reduced with higher concrete strength. In addition, using higher steel yield strength does not change the ultimate loads and strains, as well as the confinement effectiveness, but the ductility of columns is well enhanced.

- As also mentioned in the parametric study, it is worth noting that the steel tube thickness has major influence on the behavior of short circular UHPC-FSTCs under loading on concrete core. Increasing steel tube thickness can result in significant increase of ultimate loads, strain and confinement effectiveness. Therefore, among some solutions to improve the strength and the ductility of short circular UHPC-FSTCs under loading on concrete core, using thicker steel tube may be the best option.

- The simplified formulae based on the confinement index ζ for estimating the ultimate loads and strains were proposed by using the regression analysis of parametric studies from FEM and then verified by comparing with the test results by Schneider (2006). The proposed formulae provide very good predictions compared to the measured results and they can be easily used by structural engineers to design circular CFSTCs using UHPC.

- To gain clearer insight into the behavior of short circular UHPC-FSTCs under loading on concrete core, additional experimental works and numerical studies should be carried out. The FEM in ATENA-3D presented in this study can be used for the next steps with extending in the cases of using UHPC with steel fibers, slender columns, various steel thicknesses and outer diameters of steel tube, high strength steel tube and eccentric loading.

Acknowledgments

The work described in this paper was conducted by An Le Hoang as a part of his Doctoral study under the supervision of Prof. Dr.-Ing. Ekkehard Fehling. The first author would like to acknowledge the Vietnamese Government and Institute of Structural Engineering-University of Kassel, German Academic Exchange Service-DAAD for the support of his full Ph.D. scholarship.

References

- American Institute of Steel Construction (ANSI/AISC 360-10) (2010), *Specification for Structural Steel Buildings*, An American National Standard.
- An, L.H., Fehling, E. and Ismail, M. (2016), "Numerical modelling of circular concrete filled steel tube stub columns under concentric loading", *Proceedings of the HiPerMat, 4th International Symposium on Ultra-High Performance Concrete and High Performance Construction Materials*, Kassel, Germany, March.
- Architectural Institute of Japan (AIJ) (2001), *Recommendation for Design and Construction of Concrete Filled Steel Tubular Structures*, Japan.
- Cervenka, V., Jendele, L. and Cervenka, J. (2013), *ATENA Program Documentation Part 1-Theory*, Prague, Czech Republic.
- Chu, K. (2014), "Axial load behaviour of steel tube columns in-filled with various high-performance concretes", M.S. Dissertation, Ryerson University, Toronto, Canada.
- Eurocode 4 (2004), *Design of Composite Steel and Concrete Structures, Part 1-1, General Rules and Rules for Building*, British Standards Institution, London, U.K.
- Fehling, E., Leutbecher, T., Röder, F.K. and Stürwald, S. (2008), "Structural behavior of UHPC under biaxial loading", *Proceedings of the 2nd International Symposium on Ultra High Performance Concrete*, Kassel, Germany, March.
- Fehling, E., Schmidt, M., Walraven, J., Leutbecher, T. and Fröhlich, S. (2014), *Ultra-High Performance Concrete: Fundamental-Design-Example*, Wilhelm Ernst & Sohn, Verlag für Architektur und technische Wissenschaften GmbH & Co. KG, Berlin, Germany.
- Guler, S., Aydogan, M. and Copur, A. (2013), *Axial Capacity and Ductility of Circular UHPC-Filled Steel Tube Columns*, Magazine of Concrete Research.

- Han, L.H., Li, W. and Bjorhovde, R. (2014), "Development and advanced applications of concrete-filled steel tubular (CFST) structures: Members", *J. Constr. Steel Res.*, **100**, 211-228.
- Han, L.H., Yao, G.H., Chen, Z.P. and Yu, Q. (2005), "Experimental behavior of steel tube confined concrete (STCC) columns", *Steel Compos. Struct.*, **5**(6), 459-484.
- Hatzigeorgiou, G.D. (2008), "Numerical model for the behavior and capacity of circular CFT columns, part I: Theory", *Eng. Struct.*, **30**(6), 1573-1578.
- Johansson, M. (2002), "Composite action and confinement effects in tubular steel-concrete columns", Ph.D. Dissertation, Chalmers University of Technology, Göteborg, Sweden.
- Leutbecher, T. (2008), "Rissbildung und zugtragverhalten von mit fasern und stabstahl bewehrtem ultrahochfesten beton (UHPC)", Ph.D. Dissertation, University of Kassel, Germany.
- Liew, J.Y.R. and Xiong, D.X. (2010), "Experimental investigation on tubular columns infilled with ultra-high strength concrete", *Tubul. Struct. XIII*, The University of Hong Kong, Hong Kong.
- Liew, J.Y.R. and Xiong, D.X. (2012), "Ultra-high strength concrete filled composite columns for multi-storey building construction", *Adv. Struct. Eng.*, **15**(9), 1487-1503.
- Liew, J.Y.R., Xiong, M.X. and Xiong, D.X. (2014), "Design of high strength concrete filled tubular columns for tall buildings", *J. High-Rise Build.*, **3**(3), 215-221.
- Liew, J.Y.R. and Xiong, M.X. (2015), *Design Guide for Concrete Filled Tubular Members with High Strength Materials to Eurocode 4*, Research Publishing, Singapore.
- O'Shea, M.D. and Bridge, R.Q. (2000), "Design of circular thin-walled concrete filled steel tubes", *J. Struct. Eng.*, **126**(11), 1295-1303.
- Pryl, D. and Cervenka, J. (2015), *ATENA Program Documentation Part 11-Troubleshooting Manual*, Cervenka Consulting s.r.o., Prague, Czech Republic.
- Schneider, H. (2006), "Zum tragverhalten kurzer, umschnürter, kreisförmiger, druckglieder aus ungefasertem UHFB", Ph.D. Dissertation, University of Leipzig, Leipzig, Germany.
- Scholle, N. and Lohaus, L. (2012), "Numerical analyses of filigree steel-wrapped UHPC tubes", *Proceedings of the 13th Bilateral Czech/German Symposium*, Prague, Czech Republic, June.
- Song, T.Y. and Liew, J.Y.R. (2012), "Simulation model for ultra-high strength concrete filled composite column under static loads", *Proceedings of the 10th International Conference on Advances in Steel Concrete Composite and Hybrid Structures*, National University of Singapore, Singapore, July.
- Speck, K. and Curbach, M. (2011), *Mehrxiale Festigkeit von UHPC (Druck-Zug und Zug-Zug-Festigkeit)*, Vortrag in Zwischenkolloquium SPP1182, Kassel, Germany.
- Tao, Z., Wang, Z.B. and Yu, Q. (2013), "Finite element modeling of concrete filled steel stub columns under axial compression", *J. Constr. Steel Res.*, **89**, 121-131.
- Tue, N.V., Küchler, M., Schenck, G. and Jürgen, R. (2004b), "Application of UHPC filled tubes in buildings and bridges", *Proceedings of the International Symposium on Ultra High Performance Concrete*, Kassel, Germany, March.
- Tue, N.V., Schneider, H., Simesch, G. and Schmidt, D. (2004a), "Bearing capacity of stub columns made of NSC, HSC and UHPC confined by a steel tube", *Proceedings of the International Symposium on Ultra High Performance Concrete*, Kassel, Germany, March.
- Xiong, D.X. (2012), "Structural behaviour of concrete filled steel tube with high strength materials", Ph.D. Dissertation, National University of Singapore, Singapore.
- Yan, P.Y. and Feng, J.W. (2008), "Mechanical behavior of UHPC and UHPC filled steel tubular stub columns", *Proceedings of the 2nd International Symposium on Ultra High Performance Concrete*, Kassel, Germany, March.
- Yang, Z., Zhang, Y., Chen, M. and Chen, G. (2013), "Numerical simulation of ultra-strength concrete-filled steel columns", *Eng. Rev.*, **33**(3), 211-217.
- Yu, Q., Tao, Z., Liu, W. and Chen, Z.B. (2010), "Analysis and calculations of steel tube confined concrete (STCC) stub columns", *J. Constr. Steel Res.*, **66**(1), 53-64.

AW